ARTICLE

Salvianolic acid B suppresses hepatic fibrosis by inhibiting ceramide glucosyltransferase in hepatic stellate cells

Zi-bo Li[1], Lin Jiang[1], Jia-dong Ni[1], Yuan-hang Xu[1], Fang Liu[2], Wen-ming Liu[2], Shao-gui Wang[1], Zhong-qiu Liu[1] and Cai-yan Wang[1]

UDP-glucose ceramide glucosyltransferase (UGCG) is the first key enzyme in glycosphingolipid (GSL) metabolism that produces glucosylceramide (GlcCer). Increased UGCG synthesis is associated with cell proliferation, invasion and multidrug resistance in human cancers. In this study we investigated the role of UGCG in the pathogenesis of hepatic fibrosis. We first found that UGCG was over-expressed in fibrotic livers and activated hepatic stellate cells (HSCs). In human HSC-LX2 cells, inhibition of UGCG with PDMP or knockdown of UGCG suppressed the expression of the biomarkers of HSC activation (α-SMA and collagen I). Furthermore, pretreatment with PDMP (40 μM) impaired lysosomal homeostasis and blocked the process of autophagy, leading to activation of retinoic acid signaling pathway and accumulation of lipid droplets. After exploring the structure and key catalytic residues of UGCG in the activation of HSCs, we conducted virtual screening, molecular interaction and molecular docking experiments, and demonstrated salvianolic acid B (SAB) from the traditional Chinese medicine *Salvia miltiorrhiza* as an UGCG inhibitor with an IC_{50} value of 159 μM. In CCl_4-induced mouse liver fibrosis, intraperitoneal administration of SAB ($30 \, \text{mg} \cdot \text{kg}^{-1} \cdot \text{d}^{-1}$, for 4 weeks) significantly alleviated hepatic fibrogenesis by inhibiting the activation of HSCs and collagen deposition. In addition, SAB displayed better anti-inflammatory effects in CCl_4-induced liver fibrosis. These results suggest that UGCG may represent a therapeutic target for liver fibrosis; SAB could act as an inhibitor of UGCG, which is expected to be a candidate drug for the treatment of liver fibrosis.

Keywords: liver fibrosis; hepatic stellate cells; UGCG; autophagy; PDMP; salvianolic acid B

INTRODUCTION

Hepatic fibrosis is a pathophysiological process, which refers to abnormal liver proliferation caused by various injury factors. If the liver injury factors can't be removed for a long time, the process of fibrosis will develop into cirrhosis or cancer [1]. Hepatic fibrosis begins with the activation and proliferation of hepatic stellate cells (HSCs). HSCs are non-parenchymal hepatocytes, which have attracted much attention because they are the primary fibrotic cell type of liver injury [2, 3]. Activated HSCs differentiate into myofibroblasts, leading to the secretion and deposition of extracellular matrix [4]. There is increasing evidence that hepatic fibrosis is reversible. Such as elimination of activated HSC through cell death (including apoptosis, aging, autophagy, *etc.*) is considered to be an effective anti-fibrosis strategy [5]. HSCs are considered to be a plastic cell type, which can regulate liver growth, immunity, and inflammation, as well as energy and nutritional homeostasis. These functions depend on the diversity of metabolism and the strict regulation of energy consumption [6].

However, the activation or transdifferentiation of HSCs needs rapid adaptation to meet higher energy requirements. Autophagy is a cellular stress response, which participates in the autolysosomal digestion of macromolecules and organelles to produce intracellular nutrition and energy [7–9]. It is known that a key result of hydrolysis is the release of free fatty acids to "supply

energy" for cell activation. The above several activation related metabolic changes are concentrated in autophagic cells, including increased lipolysis, ROS production and ER stress [10]. Degradation of lipid droplets is a key feature of HSC activation and is driven by autophagy [11, 12]. Early studies on the effect of lipid droplet movement focused on the release of free retinol outside the cell after the hydrolysis of retinol ester in the cell [13]. At present, it is known that a key result of hydrolysis is the release of free fatty acids to "supply energy" for cell activation [14].

The latest research describes UGCG are connected to cell energy metabolisms, such as glutamine metabolism, glucose metabolism and mitochondrial function [15, 16]. In addition, UGCG might regulate fat metabolism, which indicates a role for UGCG in energy homeostasis [17]. Clinical database analysis shows that UGCG is closely related to a variety of liver diseases (Fig. 1a, b), but it is not clear whether UGCG is involved in HSC activation. UGCG is coding by the urine diphosphate-glucose ceramide glucosyltransferase gene (*UGCG*), which is located in the Golgi apparatus. The synthesis of glucosylceramide (GlcCer) catalyzed by UGCG is the first step of glycosphingolipids (GSLs) synthesis [18]. Previous research found that increased UGCG synthesis was involved in cell proliferation, migration, adhesion, angiogenesis, and multidrug resistance, etc. [19]. In liver diseases, GSLs metabolism plays an important role in

[1]Guangdong Provincial Key Laboratory of Translational Cancer Research of Chinese Medicines, Joint International Research Laboratory of Translational Cancer Research of Chinese Medicines, International Institute for Translational Chinese Medicine, Guangzhou University of Chinese Medicine, Guangzhou 510006, China and [2]School of Pharmaceutical Sciences, Guangzhou University of Chinese Medicine, Guangzhou 510006, China
Correspondence: Shao-gui Wang (wangshaogui@gzucm.edu.cn) or Zhong-qiu Liu (liuzq@gzucm.edu.cn) or Cai-yan Wang (wangcaiyan@gzucm.edu.cn)
These authors contributed equally: Zi-bo Li, Lin Jiang

Salvianolic acid B suppresses hepatic fibrosis by inhibiting UGCG
ZB Li et al.

1192

the occurrence of hepatocellular carcinoma (HCC). Recently, it has been reported that the metabolite GlcCer is required for tumorigenesis. Guri et al. found that mTORC2 promoted the lipid metabolism disorders, and resulted in hepatosteatosis and HCC [20]. Liver carcinogenesis is positively correlated with the overexpression of UGCG and the accumulation of GlcCer, and genetic or pharmacologic inhibition of UGCG can prevent HCC [21]. Activation, proliferation and transformation of HSCs are important links in various liver diseases. Here, we hypothesized that the UGCG regulates HSC activation and provides energy to support HSC activation.

In our study, we investigated the mechanism of UGCG participating in the activation of HSCs and examined the role of UGCG in HSCs activation by genetic and pharmacological inhibition and explored the mechanism of UGCG involved in HSCs activation. To explore the activity of UGCG, we obtained the uridine 5′-diphosphoglucose (UDPG)-binding domain of UGCG protein to characterize the protein of UGCG and revealed the key catalytic residues of UGCG. Through virtual screening, molecular fishing and biochemical experiment, Chinese medicine inhibitors of UGCG were found, and its anti-liver fibrosis effect was verified in vitro and in vivo.

MATERIALS AND METHODS

Reagents and antibodies
N-(1-hydroxy-3-morpholin-4-yl-1-phenylpropan-2-yl) decanamide (PDMP) (C5252, Apexbio, Houston, TX, USA) was purchased from Apexbio Biology. Chloroquine (CQ) (MB1668, Dalian, China) was purchased from Meilunbio. Salvianolic acid B (SAB) (A0056), 9′′′-MethyllithosperMate B (A0888), Lithospermate B (A0690), Gallic acid (A0110) were purchased from Manst Biotechnology (Chengdu, China). The antibodies UGCG (12869-1-AP, Proteintech, Wuhan, China), P62 (18420-1-AP, Proteintech, Wuhan, China), LC3B (18725-1-AP, Proteintech, Wuhan, China), Cathepsin L (27952-1-AP, Proteintech, Wuhan, China), TFEB (13372-1-AP, Proteintech, Wuhan, China), Flag (K200001M, Solarbio, Beijing, China), Histone-H3 (17168-1-AP, Proteintech, Wuhan, China) and β-actin (81115-1-RR, Proteintech, Wuhan, China), GAPDH (10494-1-AP, Proteintech, Wuhan, China), Keap1 (10503-2-AP, Proteintech, Wuhan, China), α-SMA (GB111364, Servicebio, Wuhan, China), Collagen I (AF7001, Affinity Biosciences, Beijing, China), and γH2AX (AF6187, Affinity Biosciences, Beijing, China) were used for Western blotting. The antibodies UGCG (sc-293235, Santa, California, CA, USA), α-SMA (G4517, Servicebio, Wuhan, China), P62 (18420-1-AP, Proteintech, Wuhan, China), LC3B (18725-1-AP, Proteintech, Wuhan, China), LAMP1 (GB4104, Servicebio, Wuhan, China), Cathepsin L (27952-1-AP, Proteintech, Wuhan, China), CD68 (GB113109, Servicebio, Wuhan, China), CD11b (GB11058, Servicebio, Wuhan, China) and γH2AX (AF6187, Affinity Biosciences, Beijing, China) were used for immunohistochemistry and immunofluorescence. The oil red staining kit (G1262, Solarbio, Beijing, China) was used for oil red staining of cells.

Animal studies and ethics statements
C57BL/6 male mice, weighing 18–22 g, were obtained from Southern Medical University (Guangzhou, China). All mice were housed at 25 °C at a humidity of 55% and on a 12 h light: dark cycle (lights on 8:00 AM to 8:00 PM) with standard rodent chow and water in an SPF animal laboratory (License number: SYXK(GZ)2019-00144) at Guangzhou University of Chinese Medicine, Guangzhou, China. All procedures were performed in strict accordance with the Guide for the Care and Use of Laboratory Animals of the China National Institutes of Health and were approved by the Institutional Animal Care and Use Committee of Guangzhou University of Chinese Medicine.

Animal administration
C57BL/6 male mice were intraperitoneally injected with CCl_4 (500 μL/kg, C805332, Macklin, Shanghai, China) diluted in corn oil (C7030, Solarbio, Beijing, China) three times a week [22]. Corn oil injection was used as a vehicle control ($n = 8$). Four weeks later, in the PDMP treatment group ($n = 8$), mice were intraperitoneally injected 20 mg/kg PDMP daily. In the SAB treatment group ($n = 8$), mice were intraperitoneally injected 30 mg/kg SAB daily [23]. The same volume of 5% tween 80 in saline was given to the mice in both the normal group ($n = 8$) and the CCl_4-induced liver fibrosis alone group ($n = 8$). After 4 weeks of treatment, mice were sacrificed, and the serum and liver tissue samples were collected for pathological analysis.

Cell culture and MTT assay
LX2 and WRL68 were purchased from the Cell Resource Center of Shanghai Institutes for Biological Sciences, Shanghai EK-Bioscience Biotechnology. Cells were cultured at 37 °C in an incubator with 5% CO_2 in DMEM (G4517, Servicebio, Wuhan, China) supplemented with 10% fetal bovine serum (12483020, Gibco, New York, NY, USA). Cell viability was determined by the MTT method, briefly, LX2 cells were seeded in 96-well plates at a density of 4×10^3/well. After treatment with PDMP at different concentrations for 48 h, cells were incubated with 20 μL, 5 mg/mL MTT (IM0280, Solarbio, Beijing, China) for 4 h, then the supernatant was removed and 100 μL DMSO was added to dissolve blue formazan crystals of viable cells. The plate was shaken for 10 min and optical density was measured using a microplate spectrophotometer at the wavelength of 570 nm.

The extraction and culture of mouse primary HSCs was based density gradient centrifugation [24]. Briefly, the Hank's buffer, 0.5% (w/v) pronase (S10014, Yuanye, Shanghai, China), and 0.044% (w/v) collagenase (GC305015, Servicebio, Wuhan, China) were sequentially perfused via superior vena cava of mouse liver. Agitation of the digested liver tissue with DNase I (R21951, Yuanye, Shanghai, China), HSCs were isolated from cell suspension with density gradient cell separation solution (P8370, Solarbio, Beijing, China). The purity of HSCs exceeds 90% as determined by fluorescence microscopy. The activated HSCs were obtained by TGF-β (50153-M08H, Sinobiological, Beijing, China) stimulation for 48 h.

Quantitative polymerase chain reaction (qPCR)
Total RNA was extracted from liver or cell samples by TRIzol reagent (GK20008-100, GLPBIO, Montclair, CA, USA). Reverse transcription was performed to obtain cDNA by using a kit (K1691, Thermo Scientific, San Jose, CA, USA). RNA levels were assessed in an ABI 7500 instrument using SYBR Green qPCR Master Mix (GK10002-1, GLPBIO, Montclair, CA, USA) and the following primers (Table 1). The relative mRNA levels were determined by the $2^{-\Delta\Delta CT}$ method with the GAPDH gene as the internal control.

Western blot
Tissue samples or cells were lysed by a mammalian lysis buffer, Bradford (5000205, BIO-RAD, Hercules, CA, USA) was used for protein quantification, equal amounts of proteins were separated

Table 1. Sequence (5′-3′) of primers used for real time quantitative PCR.

Gene	Forward (5′ → 3′)	Reverse (5′ → 3′)
Ugcg	ATGGCCTTGTTCGGCTTCG	GGTGTAACCGGGTGTAGATGAT
Gapdh	AGGTCGGTGTGAACGGATTTG	GGGGTCGTTGATGGCAACA
α-SMA	AAAAGACAGCTACGTGGGTGA	GCCATGTTCTATCGGGTACTTC
Collagen I	GAGGGCCAAGACGAAGACATC	CAGATCACGTCATCGCACAAC
RARA	AAGCCCGAGTGCTCTGAGA	TTCGTAGTGTATTTGCCCAGC
RARB	TCCGAAAAGCTCACCAGGAAA	GGCCAGTTCACTGAATTTGTCC
GAPDH	TGTGGGCATCAATGGATTTGG	ACACCATGTATTCCGGGTCAAT

Salvianolic acid B suppresses hepatic fibrosis by inhibiting UGCG
ZB Li et al.

1193

using 12% SDS-PAGE and then transferred to PVDF membrane (IPFL00010, Sigma-Aldrich, Saint Louis, MO, USA). After blocking with 5% skim milk in TBST for 2 h, it was incubated with antibodies against primary antibody overnight followed by five times washes in TBST for 5 min each. HRP-conjugated secondary anti-rabbit or anti-mouse antibodies (G1213/G1214, Servicebio, Wuhan, China) were applied for 1 h, followed by five times washes in TBST for 5 min each. Blots were incubated with ECL (MA0186-1, Meilunbio, Dalian, China). The intensity of bands was quantified using software Image J software.

Lentiviral vectors and gene transduction
For shRNA-mediated knockdown of UGCG, pLKO.1-shRNA (Youbio, Changsha, China) containing lentiviruses were used. The UGCG shRNA sequences were primers as 5′-CCGCGAATCCATGACAATA TA-3′ and 5′-GCTCAGTACATTGCCGAAGAT-3′. Lentiviruses were generated according to the manufacturer's instructions and added to the LX2 cells with 10 μg/mL polybrene (G1803, Servicebio, Wuhan, China), and incubated for 20 h with fresh growth medium. Cells were selected with 5 μg/mL puromycin (IP1280, Solarbio, Beijing, China) 2 days after the infection.

EdU assay
Cell proliferation was also determined by Ethynyl-2-deoxyuridine (EdU) incorporation assay using an EdU kit (C10310-1, Ribobio, Guangzhou, China) following the manufacturer's instructions. Briefly, cells were incubated with 100 μL of 50 μM EdU per well for 6 h at 37 °C. Then, the cells were fixed for 30 min at room temperature using 4% polyformaldehyde. Subsequently, the cells were incubated with 50 μL of 2 mg/mL glycine for 5 min followed by washing with 100 μL PBS. After permeabilization with 0.5% Triton X100, the cells were reacted with Apollo solution for 30 min. After that, cells were incubated with 100 μL Hoechst 33342 solution for 10 min followed by washing 3 times with 100 μL PBS. The cells were then visualized under a fluorescence microscopy.

Molecular cloning, site-directed mutation and transfection
The gene encoding UGCG was amplified by PCR from cDNA from human LX2 cells. The gene sequence was cloned into the pCDNA3.1-Flag vector (Youbio, Changsha, China) with the restriction sites Nhe I (FD0584, Thermo Scientific, San Jose, CA, USA) and Xho I (FD0694, Thermo Scientific, San Jose, CA, USA). The plasmid was constructed, and completely sequenced to confirm that the target sequence was inserted correctly. Rescue UGCG plasmid (rUGCG) contains non-sense mutations of C1066A, C1068A, A1071G and C1074A. The D144A, H193A, D236A and R272A mutation were generated by the Quikchange method (210519, Stratagene, Santa Clara, CA, USA) with the rUGCG plasmid as the template.

LX2 cells were seeded separately in 6-well plates. When the cell density reached 70%, the cell culture medium was replaced with serum-free and antibiotic-free Opti-MEM (31985062, Gibco, New York, NY, USA). The 2 μg plasmid and 7.5 μL Lipofectamine 3000 (L3000001, Invitrogen, Carlsbad, CA, USA) were added to the medium. After 6 h, the cell culture medium was replaced with DMEM containing 10% fetal bovine serum. After culture for 48 h, cells were harvested by scraping for subsequent experiments.

Electron microscopy
Cells were starved with serum and stimulated with 40 μM PDMP for 12 h. After fixation in 2% glutaraldehyde (G1102, Servicebio, Wuhan, China) for 30 min, cells were post-fixed in 1% Osmic acid, dehydrated and embedded in TAAB-812 resin. Ultrathin sections of 60 nM were obtained by using an ultramicrotome, and followed by uranium-lead double staining for 15 min. For correlative light and electron microscopy, cell imaging on gridded dishes, representative pictures were displayed.

Immunohistochemistry and lysosensor green stain
The cell climbing sheets were washed three times with PBS after administration, and were fixed with 4% paraformaldehyde for 30 min; then soaked in 0.1% Triton X100 (G1204, Servicebio, Beijing, China) for 5 min, and 5% BSA (GC305006, Servicebio, Wuhan, China) blocked the antigen, the primary antibody is incubated overnight at 4 °C. The cell climbing sheets are washed three times with PBS, and then incubated with CY3 or FITC conjugated secondary antibody (GB21301/GB22301, Servicebio, Wuhan, China) for 1 h at room temperature. Then, the sections were washed with PBS 3 times and incubated DAPI (GDP1024, Servicebio, Wuhan, China) and photographed with a microscope.

For lysosensor green dyestain, after 12 h of cell administration, cells were washed three times with PBS, and then cells were stained with lysosomal fluorescent probe (S34855, Gibco, New York, NY, USA) (100 ng/mL) for 5 min photographed with a microscope.

Expression and purification of UGCG protein
UGCG gene (mUGCG coding residues K39-H171, K39-D236 and K39-R272) were PCR-amplified from mouse cDNA and cloned into the pET-28a (+) expression vector with the restriction sites Nhe I and Xho I. The constructed plasmid was transfected into Escherichia coli BL21 (DE3), the recombinant proteins were initiated by 0.2 mM IPTG (RS0529, Ruishubio, Guangzhou, China) and were kept shaking overnight at 25 °C. The proteins were purified by nickel-nitrilotriacetic acid (Ni-NTA) affinity resin, and the purified proteins were characterized by 12% SDS-PAGE.

Virtual screening and molecular docking
The structure of UGCG was obtained from the protein prediction database (https://alphafold.ebi.ac.uk). The compounds with higher docking scores were screened from the traditional Chinese medicine library by Schrödinger software. Table 2 shows the top 20 traditional Chinese medicine compounds with docking scores with UGCG. The docking results were visually analyzed by Pymol software.

Surface plasmon resonance (SPR) analysis
SPR was performed on a Biacore X100 system (Biacore, GE Healthcare, Boston, MA, USA) using CM5 chip coated with the protein (mUGCG 39-272), the optimum pH for protein enrichment on the chip is 4.5. Chinese medicine compounds (SAB, 9'''- MethyllithosperMate B, Lithospermate, Gallic acid) were respectively dissolved in PBS with 0.5% DMSO, the response value of the interaction is detected according to a certain drug concentration gradient. When the response value was generated by the combination of the compound and the chip reaches saturation, the K_D value is the compound concentration corresponding to the half saturation response value.

UGCG enzyme assays
UGCG activity was measured by incubating lysate samples (equivalent to 40 μg of cell lysate) with 10 μM NBD-ceramide (C5726-1, Apexbio, Houston, TX, USA) and 2 mM UDPG (ab120384, Abcam, Cambridge, MA, USA) in enzyme assay buffer (50 mM Hepes (pH 7.4), 25 mM KCl, 5 mM MnCl$_2$), for 30 min at 37 °C, followed by lipid extraction and thin layer chromatography, and visualized by ultraviolet illumination.

Biotin labeled SAB
Aminated biotin (22.8 mg, 0.066 mM) was dissolved with N, N-dimethylformamide and triethanolamine (9.2 μL 0.066 mM) was added and stirred for 20 min, then SAB (39.8 mg, 0.055 mM) and 1-hydroxybenzotriazole (9.0 mg, 0.066 mM) were dissolved with N, N-dimethylformamide and stirred for 20 min, carbodiimide (12.7 mg, 0.066 mM) was added, and stirred at room temperature for 6 h. n-Hexane was added into the reaction system and centrifuged to obtain the lower layer of light brown liquid, it was

Salvianolic acid B suppresses hepatic fibrosis by inhibiting UGCG
ZB Li et al.

1194

Table 2. Docking scores of the top 20 compounds in virtual screening.

No.	Name/CAS	Docking score	No.	Name/CAS	Docking score
1	Salvianolic acid B 115939-25-8	−9.168	11	Salvianolic Acid C 115841-09-3	−7.456
2	9‴-MethyllithosperMate B 1167424-32-9	−8.974	12	Scutellarin 27740-01-8	−7.418
3	Safflower-yellow 36338-96-2	−8.530	13	Docetaxel 114977-28-5	−7.384
4	Lithospermate B 122021-74-3	−8.126	14	Procyanidin B2 29106-49-8	−7.363
5	lithospermic acid B 121521-90-2	−7.907	15	Parishin A 62499-28-9	−7.330
6	Glutathione 70-18-8	−7.838	16	2′-acetylacteoside 94492-24-7	−7.318
7	Gallic acid 149-91-7	−7.781	17	Kaempferol 3-gentiobioside 22149-35-5	−7.307
8	1,2,3,4,6-O-Pentagalloylglucose 14937-32-7	−7.552	18	Carboxyatractyloside tripotassium salt 77228-71-8	−7.216
9	Secoisolariciresinol diglucoside 148244-82-0	−7.547	19	lithospermic acid 28831-65-4	−7.188
10	Hydroxysafflor yellow A 78281-02-4	−7.502	20	Nuezhenide 39011-92-2	−7.180

transferred and concentrated under reduced pressure. Finally, the biotin labeled SAB was separated by high performance liquid chromatography and identified by nuclear magnetic resonance.

Molecular fishing
We used biotin-labeled SAB and incubated it with LX2 cell lysates for 2 h, and then isolated the protein bound to SAB with streptavidin magnetic beads (M2422, Solarbio, Beijing, China). The binding proteins were eluted with SDS loaded dyes, analyzed by SDS-PAGE, and then visualized by silver stain (G7210, Solarbio, Beijing, China), then SAB-binding proteins were identified by Oebiotech (Shanghai, China) using mass spectrometry.

Liver histology, biochemical analysis and immunohistochemistry
The liver tissue was fixed in 4% formalin buffer (G1101, Servicebio, Wuhan, China) for 24 h and embedded in paraffin. Sections (5 mm thick) were cut and stained with hematoxylin, eosin and masson. ALT (MM-44625), AST (MM-44115), IL-6 (MM-0163) and IL-1β (MM-0040) were determined by ELISA kits, and the ELISA kits were purchased from Meimian Biotechnology (Yancheng, China), according to the manufacturer's protocols. The content hydroxyproline in liver tissues was determined hydroxyproline assay kit (A030-2-1, Jiancheng Bioengineering Institute, Nanjing, China). Immunohistochemical staining was performed using immunohistochemical kit (G1215, Servicebio, Wuhan, China). Photographs were taken in a blinded fashion at random fields, and representative pictures of liver sections were displayed.

Statistical analysis
The data were statistically analyzed were performed using GraphPad Prism 7 and presented as the mean ± SD. Differences in mean values between groups were analyzed by two-sided Student's t test.

RESULTS
UGCG expression was up-regulated in liver fibrosis
UGCG has been described to be significantly elevated in HCC, the expression of UGCG in other liver diseases has not been elucidated so far. The publicly available GEO datasets with Affymetrix microarray measurements (GSE28619) showed that UGCG was significantly up-regulated in alcoholic hepatitis (Fig. 1a). Oncomine database (https://www.oncomine.com/) showed that UGCG expression was significantly up-regulated in liver cirrhosis (Fig. 1b). In CCl_4 induced-liver fibrosis model mice, UGCG was significantly up-regulated in transcription (Fig. 1c) and protein level (Fig. 1d, e). The activation of HSCs was the central event in the occurrence and development of various liver diseases. We extracted mouse HSCs, and our results showed that UGCG and α-SMA were up-regulated after the

activation of HSCs by TGF-β (Fig. 1f, g). These data suggested that UGCG may be involved in the activation of HSCs. UGCG is a glycosyltransferase involved in the first step of GSLs synthesis, its catalytic product GlcCer can be catalyzed by B4galt5 to produce lactosylceramides, and then further metabolized to produce more complex GSLs (Fig. 1h).

The inhibition of UGCG suppressed the activation of HSCs
We used human HSC-LX2 cell to explore the effect of UGCG inhibition on HSCs activation, and two strategies were used to inhibit UGCG. One strategy is using PDMP, an inhibitor of UGCG [25], to inhibit the activity of UGCG, the other strategy is using shRNA to knockdown UGCG (Fig. 2a). MTT assay showed that PDMP significantly inhibited LX2 cell viability in a dose-dependent manner (IC_{50}: 62.8 μM) and had a low effect on WRL68 normal liver cells (Fig. 2b). Under a microscope, we found PDMP promoted the formation of intracellular vesicles (Fig. 2c). It is generally believed that HSC activation is the main cause of liver fibrosis, followed by excessive synthesis and deposition of collagen liver in fibrotic tissue. Our results showed that PDMP inhibited the expression of α-SMA and Collagen I in a dose-dependent manner (Fig. 2d, e). In order to further confirm that the suppression of UGCG could inhibit the activation of HSCs, we used shRNA to interfere with the expression of UGCG. EdU experiment showed that the knockdown of UGCG could significantly inhibit the proliferation of cells (Fig. 2f), and the activation markers of HSC were also significantly down-regulated (Fig. 2g). The inhibitory effect of shRNA-1 was more obvious. In addition, we treated cell with 2 μM UGCG product GlcCer after PDMP treatment, the expression of α-SMA was partly rescued, and GlcCer alone had no effect on the expression of α-SMA (Fig. 2h). We constructed rUGCG to avoid the interference of shRNA, and rescued rUGCG to the cells on the basis of UGCG knockdown. The results showed that the expression of α-SMA could be rescued by rUGCG (Fig. 2i).

UGCG inhibition blocked autophagy flow in HSCs
The changes in intracellular vesicle structure and function of HSCs are closely related to its activation. We observed HSCs by transmission electron microscope, compared with the control group, the number of autophagosomes increased and deformity occurred in cells treated with PDMP (Fig. 3a). Next, we explored the expression of autophagy markers LC3B and P62 after PDMP treated cells, we evaluated the time course of autophagy in response to PDMP in LX2 cells. LX2 cells were treated with 40 μM of PDMP for 0, 3, 6, 12, and 24 h, respectively. PDMP treatment could promote the increase of LC3B-II and P62 and the effect reached the maximum at 12 h (Fig. 3b). Besides, PDMP could increase LC3B-II and P62 in a dose-dependent manner (Fig. 3c). Compared with autophagy inhibitor chloroquine (CQ), PDMP worked in a similar way as CQ (Fig. 3d). Meanwhile,
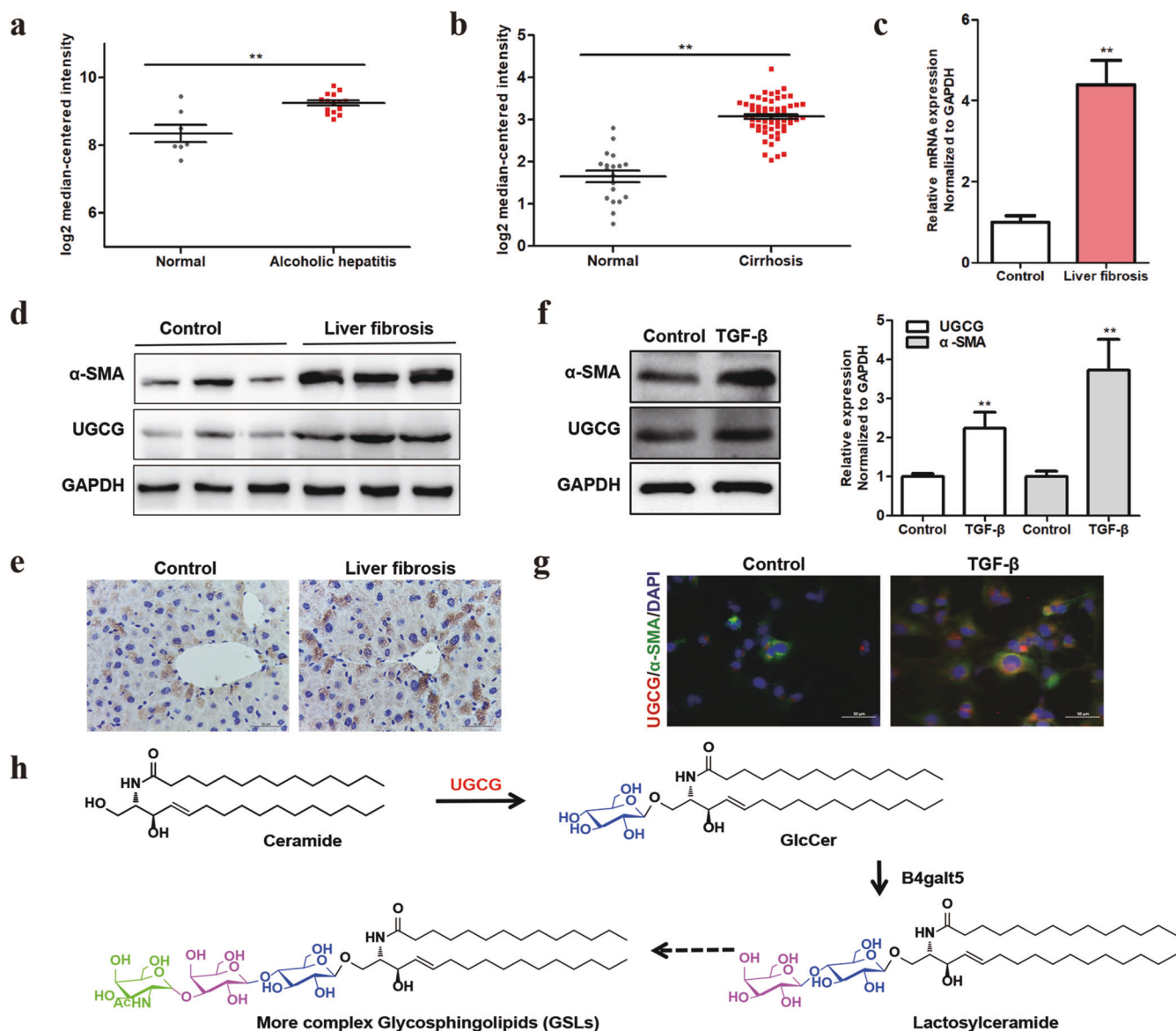
Salvianolic acid B suppresses hepatic fibrosis by inhibiting UGCG
ZB Li et al.

1195

Fig. 1 The expression of UGCG is up-regulated in hepatic diseases, especially hepatic fibrosis. a Comparison of UGCG expression in normal tissues and alcoholic hepatitis. **b** Comparison of UGCG expression in normal tissues and cirrhosis. The mRNA (**c**) and protein (**d**) expression of UGCG in the control group and CCl$_4$-induced liver fibrosis group. **e** Immunohistochemical staining of UGCG in mouse liver tissues. The expression of UGCG and α-SMA were evaluated by Western blot (**f**) and immunofluorescence (**g**) in mouse HSCs. **h** Schematic diagram of GSLs metabolism. The experiments were repeated three times, and statistical significance was determined by a *t*-test. *$P < 0.05$, **$P < 0.01$.

immunofluorescence method was used to verify the similar effect of PDMP on LC3B-II and P62 expression (Fig. 3e). Besides, we used 2 μM UGCG product GlcCer to treat cells, the increase of LC3B-II and P62 induced by PDMP were partially rescued (Fig. 3f). These data suggested that the inhibition of UGCG could block the autophagy process in the late stage.

The inhibition of UGCG impaired lysosomal homeostasis and degradation function
The late inhibition of autophagy is closely related to the function of lysosomes. Then we used double immunofluorescence staining to locate autophagosomes and lysosomes. After PDMP treatment of LX2 cells for 24 h, autophagosome marker LC3B increased, but LAMP1 did not change significantly. The two fluorescence could not fuse well. However, after CQ treatment, autophagosome accumulation increased and fused with lysosomes, GlcCer could rescue the effect of PDMP, but not CQ (Fig. 4a). The fluorescence

of lysotracker decreased after PDMP treatment, and had a similar effect with CQ, this result suggested that inhibition of UGCG could change the pH of lysosomes (Fig. 4b). Cathepsin L was released from lysosome to cytoplasm when the lysosomal membrane permeability was damaged [26]. Our results showed that the cleavage of Cathepsin L decreased after PDMP treatment (Fig. 4c). Immunofluorescence also showed that the granular distribution of Cathepsin L was changed to dispersion by the treatment of PDMP (Fig. 4d). Besides, we found that TFEB increased in nucleus (Fig. 4e). All these proved that lysosomal membrane homeostasis was impaired. The degradation function of lysosome was closely related to the activation of HSCs. The metabolomic analysis showed that PDMP could decrease the level of GlcCers, through KEGG enrichment of differential metabolites, we found PDMP could regulate the metabolism of vitamin A signaling pathway (Fig. 4f). Lipid droplets were the main storage sites for retinoic acid, and we speculated that the impairment of lysosomal
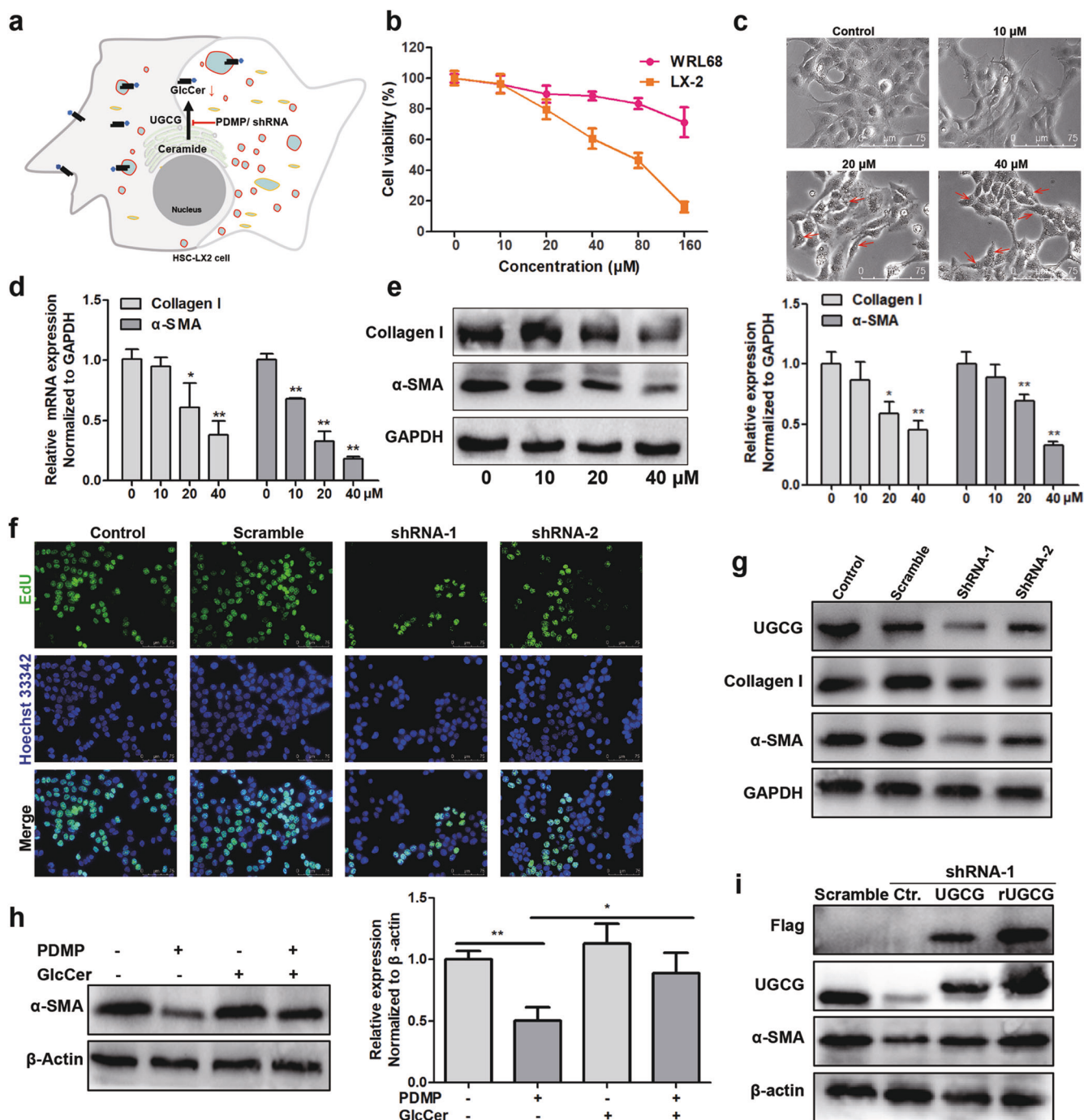
Salvianolic acid B suppresses hepatic fibrosis by inhibiting UGCG
ZB Li et al.

1196

Fig. 2 The inhibition of UGCG suppresses the activation of HSCs in vitro. a Schematic diagram of strategy for intervention of UGCG. **b** MTT assay of PDMP-treated WRL68 or LX2 cells for 48 h. **c** Cell morphology assessment, red arrows indicate the representative intracellular vesicles. **d** The mRNA levels of Collagen I and α-SMA after treatment of cells with different PDMP concentrations, as detected by qPCR. **e** The protein levels of Collagen I and α-SMA were detected by Western blot. **f** The effect of UGCG knockdown on the proliferation of LX2 cells, as detected by an EdU kit. **g** The expression levels of UGCG, Collagen I and α-SMA were evaluated by Western blot. **h** Effect of exogenous GlcCer (2 μM) on the expression of α-SMA. **i** UGCG knockdown cells were rescued with UGCG or rUGCG. The experiments were repeated three times, and statistical significance was determined by a t-test. *$P < 0.05$, **$P < 0.01$.

function caused by UGCG inhibition could block the degradation of lipid droplets and retinoic acid (Fig. 4g). Oil red staining showed that both PDMP and CQ could promote the accumulation of lipid droplets in cells, but the effect of CQ couldn't be rescued by GlcCer (Fig. 4h). Besides, we detected the changes of retinoic acid signal in cells and found that autophagy inhibition caused by PDMP could promote the expression of RARA and RARB (Fig. 4i).

The structure of UGCG was essential in the activation of HSCs UGCG protein is a transmembrane protein (Fig. 5a). The full-length protein is difficult to express and purify in a variety of expression systems, so there is little research on the structure of UGCG at present. Fortunately, we obtained the UDPG binding domain of UGCG in the expression system of *E. coli*. After many attempts, we did not obtain the crystal structure of UGCG, but we found that UGCG short fragments were easy to form dimer in solution. In
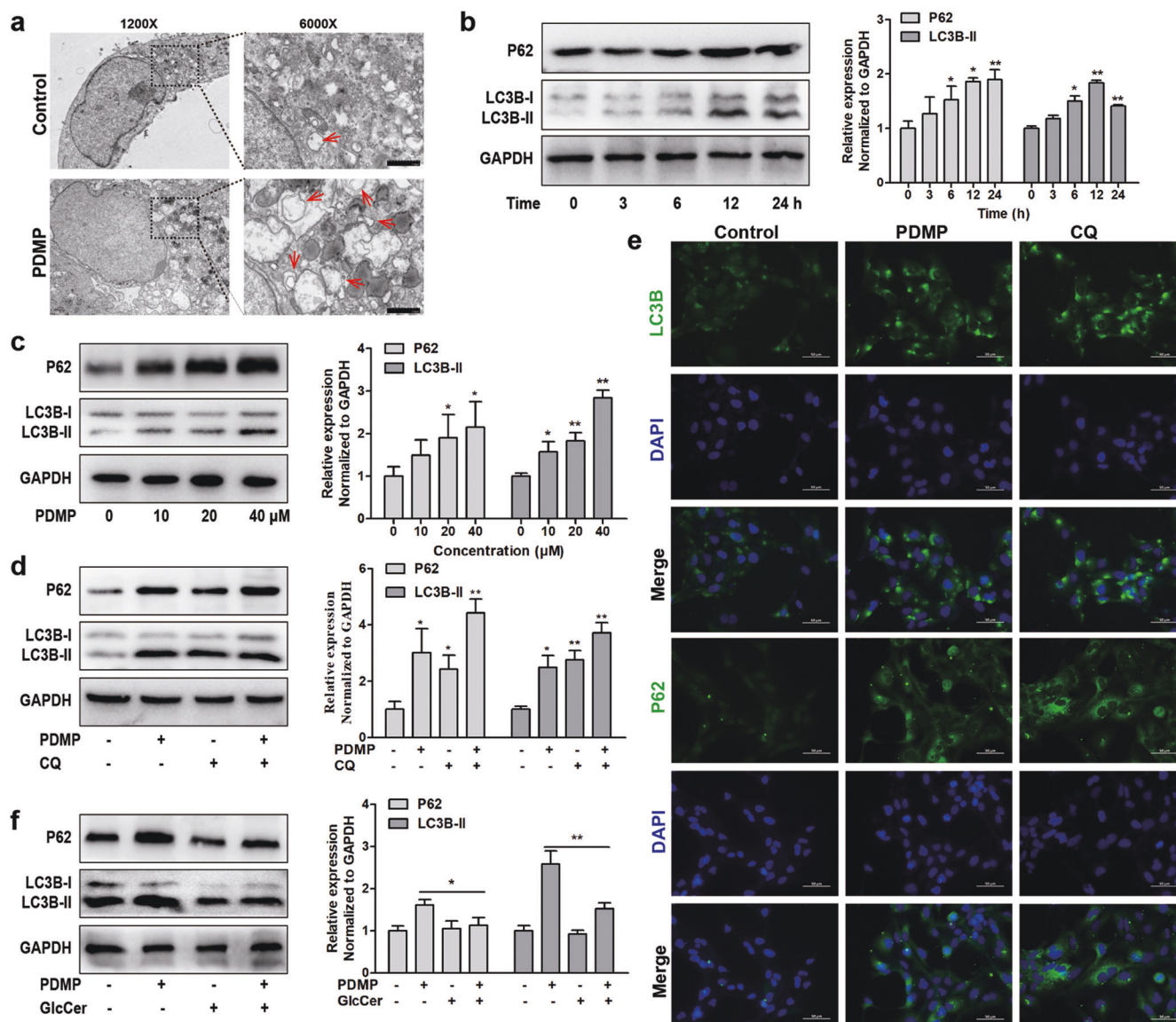
Salvianolic acid B suppresses hepatic fibrosis by inhibiting UGCG
ZB Li et al.

1197

Fig. 3 The inhibition of UGCG blocks autophagy flow. a Human HSC-LX2 cells were pretreated with 40 μM PDMP for 12 h and microstructure of cell was analyed by transmission electron microscopy, red arrows indicated autophage (Scale bar, 1 μm). **b** The expression levels of LC3B and P62 were evaluated in different time periods by Western blot. **c** The expression levels of LC3B and P62 were evaluated by Western blot analysis in LX2 cells treated with different concentrations of PDMP. **d** The expression levels of LC3B and P62 were evaluated by Western blot analysis in LX2 cells treated with PDMP (40 μM), CQ (20 μM), or CQ (20 μM) + PDMP (40 μM). **e** The expression levels of LC3B and P62 were evaluated by immunofluorescence analysis in LX2 cells treated with PDMP (40 μM) or CQ (20 μM). **f** The expression levels of LC3B and P62 were evaluated by Western blot analysis in LX2 cells treated with PDMP (40 μM), GlcCer (2 μM), or GlcCer (2 μM) + PDMP (40 μM). The experiments were repeated three times, and statistical significance was determined by a *t*-test. *$P < 0.05$, **$P < 0.01$.

solution, with presence of reducing agent dithiothreitol (DTT), the dimer decreased, and monomer increased (Fig. 5b). Meanwhile, the result from Coomassie Brilliant Blue stain consisted with the gel filtration (Fig. 5c, d). Through prediction, we speculated that the formation of dimer was related to C143 (Fig. 5e). After protein cross-linking with glutaraldehyde, UGCG was easy to form polymers in cells (Fig. 5f), this phenomenon may be related to the redox state in vivo. To explore the catalytic mechanism of UGCG, we compared the sequences of the UGCG in different species; through the conservative analysis of the secondary structure and three-dimensional structure of UGCG (Fig. 5g, h), we found that there were several key residues (D144, H193, D236, R272) in the UDPG binding domain of UGCG. We verified whether the mutation of these key residues were related to the activation of HSCs in cell experiments. The mutant

plasmids were constructed and transfected into LX2 cells with UGCG knockdown, and the result showed that the mutation of D144A and D236A had less rescue effect on α-SMA expression, which pointed out aspartic acid was important for glucosyl-transferase (Fig. 5i).

SAB inhibited UGCG and regulated the activation of HSCs
Traditional Chinese medicine plays an important role in the process of anti-liver fibrosis, but UGCG currently has no inhibitors derived from Chinese medicine. Through virtual screening, we found that there were a variety of Chinese medicine ingredients could combine with UGCG (Table 2), especially some of the pharmacodynamic ingredients of *Salvia miltiorrhiza* were in the top 10, which explained the insight target of anti-liver fibrosis from other research based on *Salvia miltiorrhiza*. We further verified these components interacted
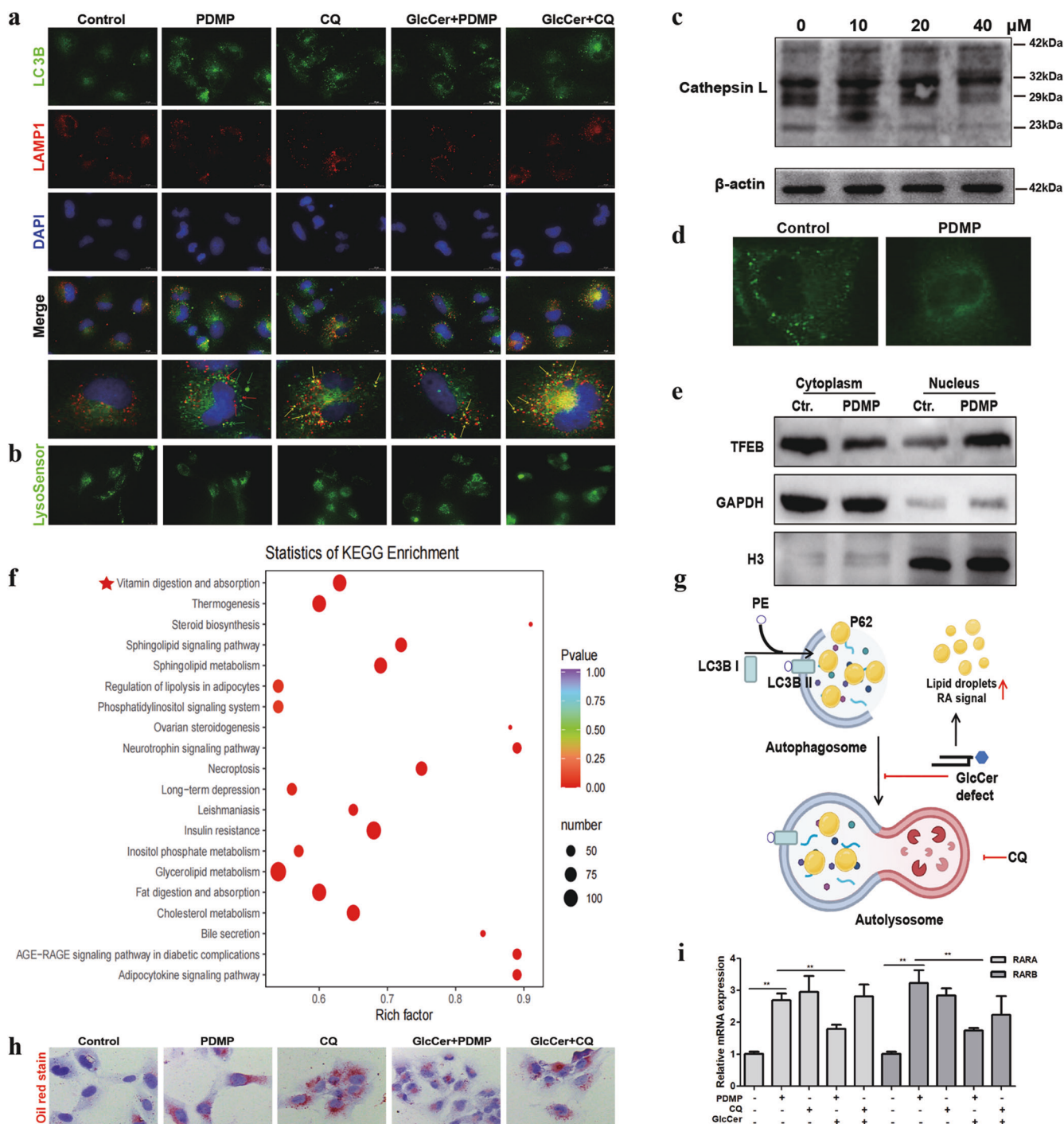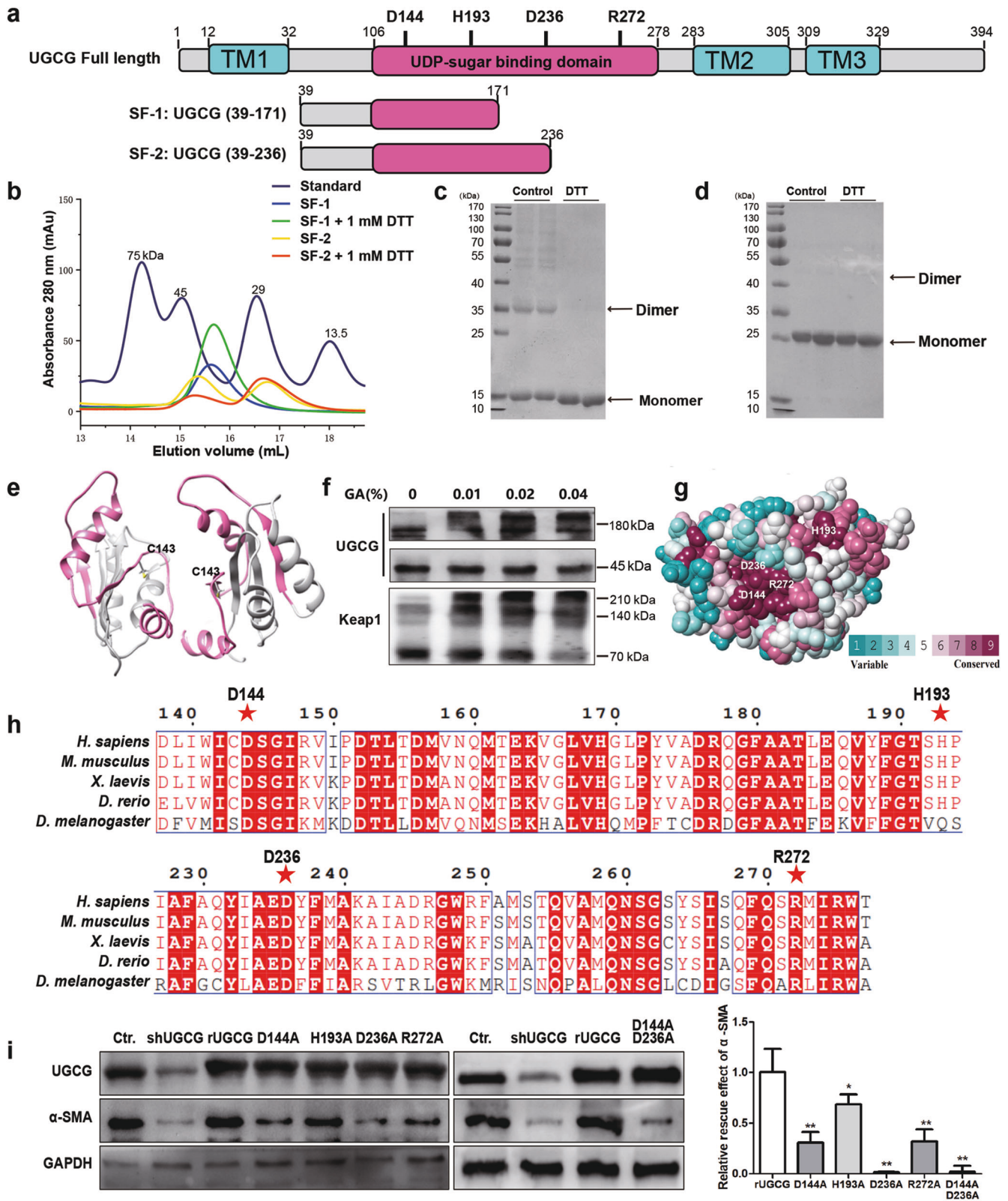
Salvianolic acid B suppresses hepatic fibrosis by inhibiting UGCG
ZB Li et al.

1198

Fig. 4 **The inhibition of UGCG impairs lysosomal homeostasis and promotes lipid droplet accumulation. a** The expression of LC3B, LAMP1 in LX2 cells were detected by immunofluorescence staining. **b** Lysosomal pH was detected by LysoSensor probe. **c** The maturation of Cathepsin L, after treat with PDMP was verified by Western blot. **d** Fluorescence images of cells were measured by antibody against Cathepsin L. **e** After PDMP treatment, the distribution of TFEB in cytoplasm and nucleus was detected by Western blot. **f** Intracellular differential lipid metabolites after PDMP treatment were used for KEGG signaling pathway analysis. **g** Schematic diagram of lysosomal imbalance caused by GlcCer defect. **h** The effect of PDMP on intracellular lipid droplets was observed by oil red staining. **i** The relative mRNA expression of RARA and RARB was detected by qPCR. The experiments were repeated three times, and statistical significance was determined by a t-test. **$P < 0.01$.

with UGCG using SPR technology, the analysis results showed that the affinity of SAB, 9′′′-MethyllithosperMate B, Lithospermate B, Gallic acid were 138 μM, 194 μM, 3.622 mM and 126 μM, respectively (Fig. 6a–d), we used the UDPG domain of UGCG, so we didn't obtain high affinity. Cell experiments also showed that SAB and

Gallic acid had strong inhibitory effect on cell viability in LX2 cells (Fig. 6e). Further we detected the effect of SAB and Gallic acid on the expression of LX2 activation markers, the results of Western blot showed that SAB could effectively inhibit the expression of α-SMA at 50 μM (Fig. 6f). To confirm the direct interaction, we used biotin-

Salvianolic acid B suppresses hepatic fibrosis by inhibiting UGCG
ZB Li et al.

1199

a UGCG Full length — domain map with TM1 (12–32), UDP-sugar binding domain (106–278) with marks D144, H193, D236, R272, TM2 (283–305), TM3 (309–329), full length 1–394. SF-1: UGCG (39–171). SF-2: UGCG (39–236).

b Absorbance 280 nm (mAu) vs Elution volume (mL). Standard, SF-1, SF-1 + 1 mM DTT, SF-2, SF-2 + 1 mM DTT. Peaks: 75 kDa, 45, 29, 13.5.

c and **d** Control/DTT gels with Dimer and Monomer bands.

e Structural cartoon with C143.

f GA(%): 0, 0.01, 0.02, 0.04. UGCG 180 kDa, 45 kDa. Keap1 210 kDa, 140 kDa, 70 kDa.

g Space-filling model colored Variable (1) to Conserved (9), labels D144, D236, R272, H193.

h Sequence alignment of H. sapiens, M. musculus, X. laevis, D. rerio, D. melanogaster with marks D144, H193, D236, R272.

i Western blots: Ctr., shUGCG, rUGCG, D144A, H193A, D236A, R272A, D144A D236A for UGCG, α-SMA, GAPDH. Bar graph: Relative rescue effect of α-SMA.

labeled SAB incubated with LX2 cell lysates and pulled down with streptavidin beads, the SAB-binding protein was visualized by silver stain (Fig. 7a, b) and identified by mass spectrometry. The results showed that 708 proteins interacted with SAB, and UGCG is one of them (Fig. 7c). Molecular docking showed that the hydrogen interaction from two important residues D236 and R272 involved in catalysis could be destroyed by phenolic hydroxyl of SAB (Fig. 7d). The mutation of D236A and R272A could reduce the production of NBD-C6-GlcCer, and lead to a decrease of 95% and 80% of activity of UGCG, respectively (Fig. 7e). The enzyme activity experiment showed that SAB could inhibit the activity of UGCG, the IC_{50} was 159 μM (Fig. 7f, g).

Salvianolic acid B suppresses hepatic fibrosis by inhibiting UGCG
ZB Li et al.

1200

Fig. 5 Study on protein structure and activity of UGCG. a Domain organization of UGCG, with boundaries indicated. The transmembrane domain (TM) and UDPG binding domain are colored in blue and red. **b** The gel filtration running trace of SF-1 and SF-2 with a Superdex 200 increase column, superimposed on the chromatogram of standard protein markers. **c** and **d** SDS-PAGE analysis of purified SF-1 and SF-2 with or without 1 mM DTT by coomassie blue staining. **e** The predicted dimer of UGCG. **f** UGCG protein in LX2 cells was crosslinked with glutaraldehyde, and Keap1 was used as positive control. **g** Sequence conservation analysis of UGCG (the conservations scales were shown in lower right). **h** Multiple sequence alignment was performed for Homo sapiens (*H. sapiens*), Mus musculus (*M. musculus*), Danio rerio (*D. rerio*) and Drosophila melanogaster (*D. melanogaster*) for UDPG binding domain of UGCG. **i** Rescue effect of different mutants of UGCG was evaluated by Western blot. The experiments were repeated three times, and statistical significance was determined by a *t*-test. *$P < 0.05$, **$P < 0.01$.
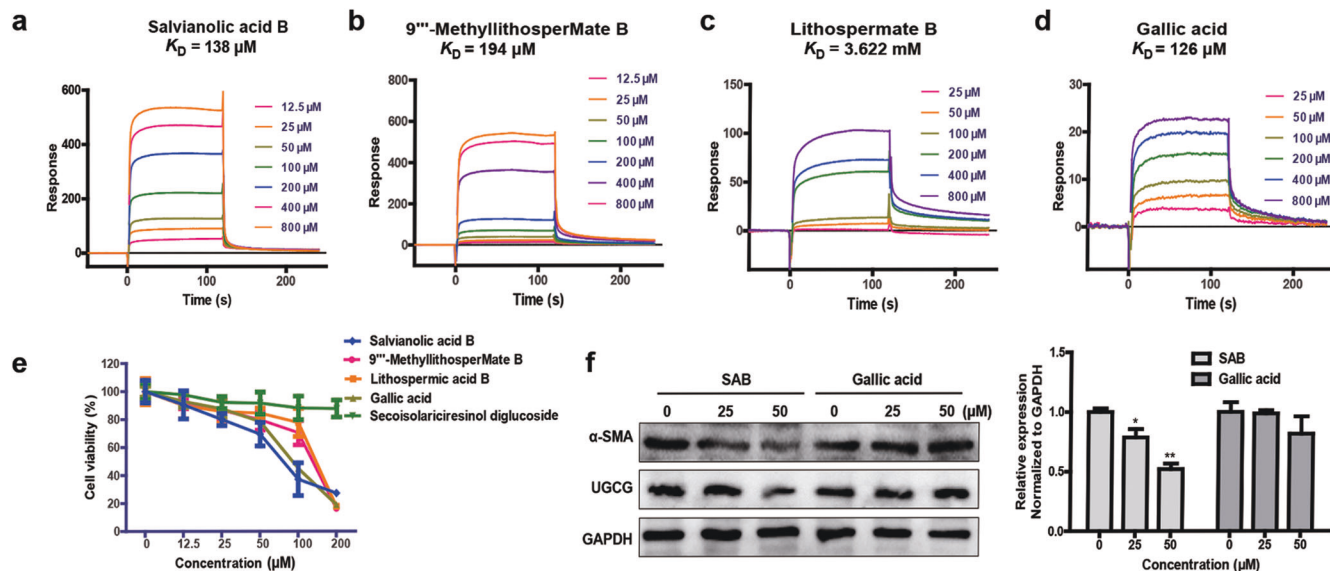

Fig. 6 Screening of potential inhibitors from traditional Chinese medicine for UGCG. a–d The affinity of UGCG with different components were detected by Biacore. **e** The viability of LX2 cells treated with different components was detected by MTT assay. **f** The expression levels of α-SMA were evaluated by Western blot analysis. The experiments were repeated three times, and statistical significance was determined by a *t*-test. *$P < 0.05$, **$P < 0.01$.

The inhibition of UGCG alleviated CCl₄-induced liver fibrosis

In order to verify the therapeutic effect of UGCG inhibitor on liver fibrosis, we used CCl₄-induced liver fibrosis model and detected the anti-fibrosis effect of the two drugs 4 weeks after administration. The modeling and treatment scheme were shown in Fig. 8a. Finally, after sacrificing mice, we found that CCl₄ could lead to lipid deposition and roughness on the liver surface (Fig. 8d). The liver index of CCl₄ group was 6.95 ± 0.49, indicating that the liver of mice proliferated. While the liver index decreased, and the surface roughness decreased after PDMP and SAB treatment (Fig. 8b). Meanwhile, the level of hydroxyproline in liver tissue was also down-regulated (Fig. 8c). We also detected the content SAB in the liver after administration to ensure that SAB plays its role (Fig. 8e). Analysis of histopathological sections showed that CCl₄ group had severe hepatic fibrosis texture and collagen deposition, while PDMP and SAB treatment had a good therapeutic effect on hepatic fibrosis, among which PDMP had a more obvious effect on inhibiting hepatic fibrosis and collagen deposition (Fig. 8f, g). We also detected the activation markers of HSCs in mice, the results showed that PDMP could significantly inhibit the expression of HSCs activation markers α-SMA and Collagen I, while SAB had a weaker effect on the activation of HSCs than PDMP (Fig. 8h, i). Besides, after CCl₄ induced liver fibrosis, LC3B and P62 tended to decrease, and LC3B-II and P62 increased significantly after PDMP and SAB treatment (Fig. 8j).

The inhibition of UGCG alleviated CCl₄-induced liver inflammatory

Anti-inflammatory activity and anti-injury effect are also important indexes to evaluate the therapeutic effect of drugs. Compared with the CCl₄ group, PDMP and SAB could significantly reduce the levels of ALT and AST in mice (Fig. 9a). CCl₄-induced liver fibrosis and also caused severe inflammatory response, the level of IL-1β and IL-6 reached 80.13 ± 4.67 pg/mL and 102.09 ± 4.81 pg/mL, respectively. Both PDMP and SAB inhibited IL-1β and IL-6 expression, and IL-6 decreased more significantly after SAB treatment (Fig. 9b). In addition, we further studied whether the two drugs affected the activation of liver Kuffer cells, CCl₄ induced a significant increase of CD68 and CD11b cell in liver, after SAB treatment, the infiltration of these immune cells was significantly reduced, while the effect of PDMP was weak (Fig. 9c). CCl₄-induced liver fibrosis is associated with severe liver DNA damage, the markers of liver DNA damage γH2AX decreased significantly after treatment with SAB and PDMP, and their anti-liver DNA damage effect was equal (Fig. 9d). Meanwhile, immunofluorescence method was used to verify the similar effect of γH2AX (Fig. 9e). In general, both PDMP and SAB could reduce the damage, inflammation and fibrosis caused by CCl₄, SAB had obvious advantages in inhibiting the activation of Kuffer cells.

DISCUSSION

The correlation between GSLs metabolism and liver diseases has attracted more and more attention. As a key enzyme in the synthesis of GSLs, the role of UGCG in liver diseases has been reported in many cases. Hepatic sphingomyelin synthase 1 deficiency could lead to steatosis, steatohepatitis, fibrosis, liver fibrosis and tumorigenesis, the main reason for this pathological process was the accumulation of GlcCer caused by the deficiency of sphingomyelin synthase 1 [27]. Jennemann et al. found that UGCG repression with siRNA decreased the level of GSLs
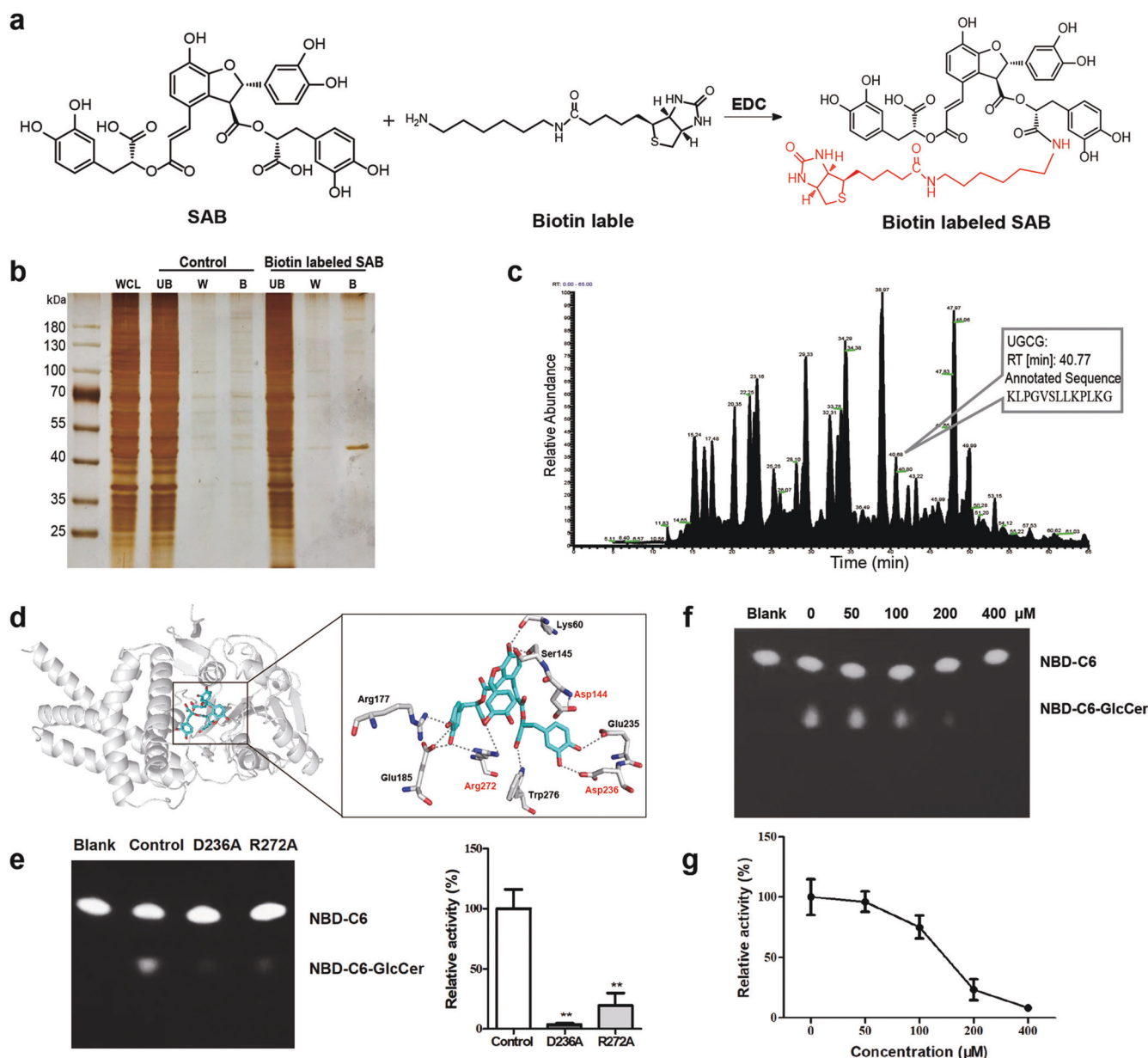
Salvianolic acid B suppresses hepatic fibrosis by inhibiting UGCG
ZB Li et al.

1201

Fig. 7   Salvianolic acid B targets UGCG. a The chemical structural formula of biotin-labeled SAB. **b** SAB-binding proteins were visualized by silver staining. WCL: whole cell lysates, UB: the unbound proteins, W: the washing proteins, B: SAB-binding proteins. **c** Total Ion Current (TIC) chromatograms from 4 to 65 min. **d** Molecular docking of SAB with UGCG, hydrogen bonds formed within 3.5 Å. **e** The activity of UGCG mutations was detected by thin layer chromatography. **f** and **g** The activity of UGCG was detected by thin layer chromatography. The experiments were repeated three times, and statistical significance was determined by a t-test. $*P < 0.05$, $**P < 0.01$.

in plasma membrane, which led to a delay of cytokinesis in hepatoma cells. In the mouse model of liver cancer, UGCG deficiency resulted in the deletion of GSLs, and significantly delayed diethylnitrosamine-induced life-threatening tumor burden [21]. It is reported that GlcCer had accumulated in the early stage of hepatocarcinogenesis, which suggested that GlcCer may be related to early liver diseases [20]. Through the collation and analysis of clinical data, we found that UGCG was up-regulated in many liver diseases. Our study found that UGCG was closely related to liver fibrosis, and up-regulated once HSCs were activated. In vitro experiments, the activation markers Collagen I and α-SMA of HSCs were down-regulated after treated with PDMP or shRNA, and cell proliferation was also inhibited. In addition, the rescue experiment also confirmed that the inhibition of UGCG could regulate the activation of HSCs. Taken together, our results suggested UGCG might be a potentially therapeutic target for live fibrosis.

It is well known that the imbalanced synthesis and degradation of extracellular matrix ultimately results in liver fibrosis and cirrhosis [28, 29]. Extracellular matrix-producing myofibroblasts in liver are predominantly derived from the activated HSCs [30]. The enhancement of autophagy is a key factor in the activation of HSCs, it is reported that TGF-β1 induced autophagy activates HSCs via the ERK and JNK signaling pathways [31]. Deng et al. also found hypoxia and LPS-induced autophagy and activation of HSC by HIF1α [32]. Chen et al. demonstrated that LPS exposure promotes HSC fibrosis through increased autophagy activity and dysfunctional retinoic acid signaling, this novel mechanism underlying the LPS-induced fibrosis response of HSCs was associated with lipid droplets loss and the TGF-β signal downregulation [33]. GSLs are also involved in the
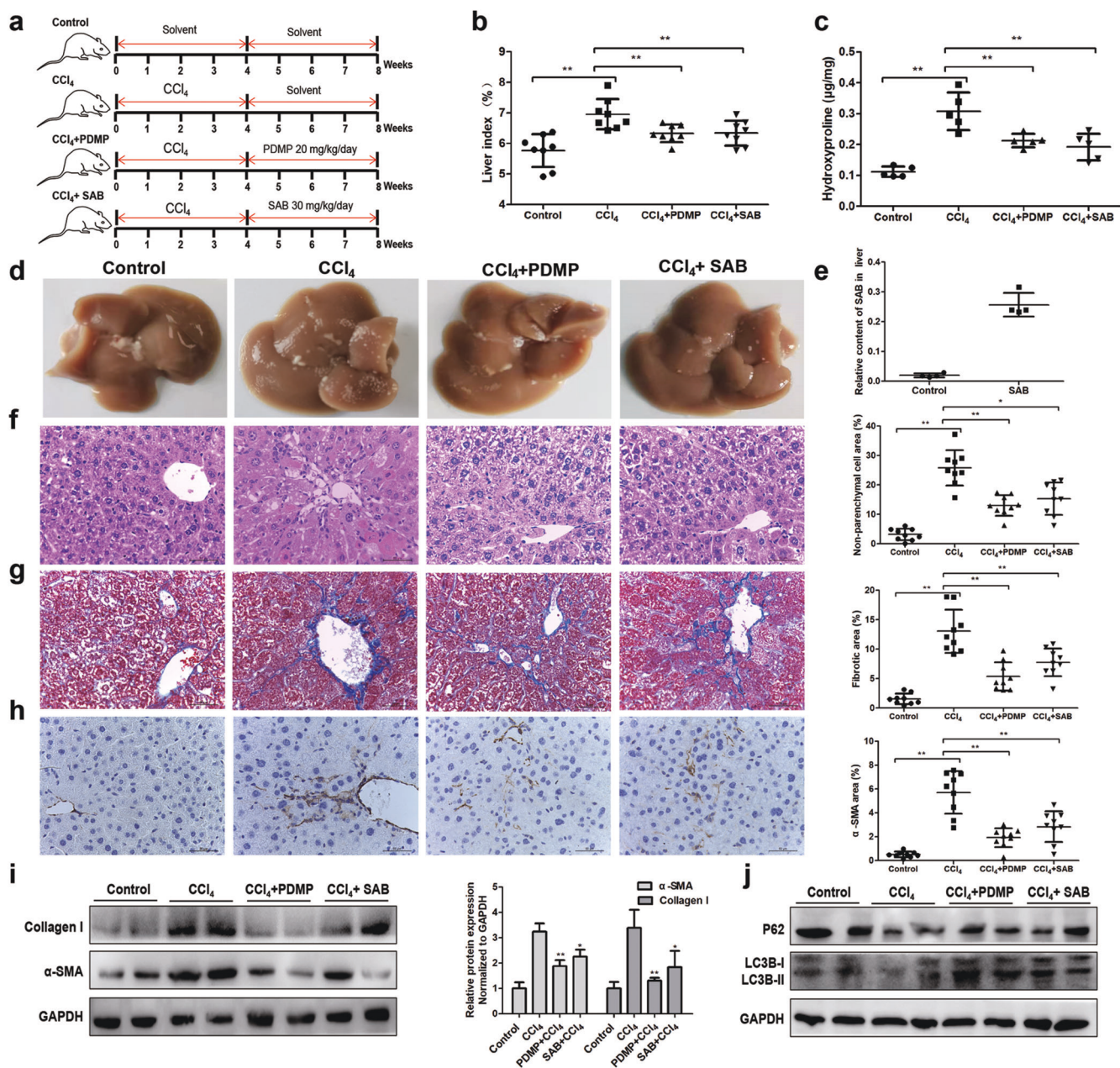
Salvianolic acid B suppresses hepatic fibrosis by inhibiting UGCG
ZB Li et al.

1202

Fig. 8 **The inhibition of UGCG ameliorates CCl4-induced hepatic fibrogenesis. a** Timeline of CCl_4-induced hepatic fibrosis and administration of PDMP and SAB. **b** Liver index statistics of mice in each group. Each group contained at least 6 mice. **c** The content of hydroxyproline in mouse livers. **d** The appearance of liver tissues in the different groups of mice. **e** The relative content of SAB in liver was detected by mass spectrum. H&E staining (40×, scale bar, 50 μm) (**f**) and Masson staining (**g**) (40×, scale bar, 50 μm) of liver tissue of mice in different groups. **h** Immunohistochemical detection of α-SMA protein expression in mice liver tissues (40×, scale bar, 50 μm). **i** Relative protein levels of α-SMA and Collagen I in mice livers, as measured by Western blot. **j** Relative protein levels of P62 and LC3B in mice livers, as measured by Western blot. The experiments were repeated three times, and statistical significance was determined by a t-test. *$P < 0.05$, **$P < 0.01$.

regulation of autophagy, in Gaucher disease, the accumulation of GSLs caused the destruction of lysosomal function and hindered the autophagy process [34]. GlcCer and lactosylceramide also participated in the autophagy process of lung endothelial cells, and the blockage of GSLs synthesis by cigarette smoke accelerated the process of emphysema [35, 36]. In our study, we found that UGCG inhibition with PDMP impaired lysosomal homeostasis, and the autophagosomes were unable to fuse with lysosomes, leading to the increase of intracellular lipid droplets and activation of retinoic acid signaling pathway in HSCs. Whereas GlcCer treatment rescued the increase of lipid droplets and retinoic acid signals in response to

PDMP exposure. Consistent with our research, Hartwig et al. found that PDMP caused lysosomal lipid accumulation [37]. Many compounds acted by inhibiting autophagy in HSCs [38, 39]. Meng et al. found that carvedilol suppressed autophagy and promoted apoptosis in HSCs via the late-stage inhibition of autophagy [40]. Our results showed that the inhibition of UGCG could block the process of autophagy, and led to the accumulation of lipid droplets and activation of retinoic acid signaling pathway.

The biochemical study of UGCG has been difficult because the full-length protein has never been completely purified. Early studies found that human and mouse UGCG could be expressed
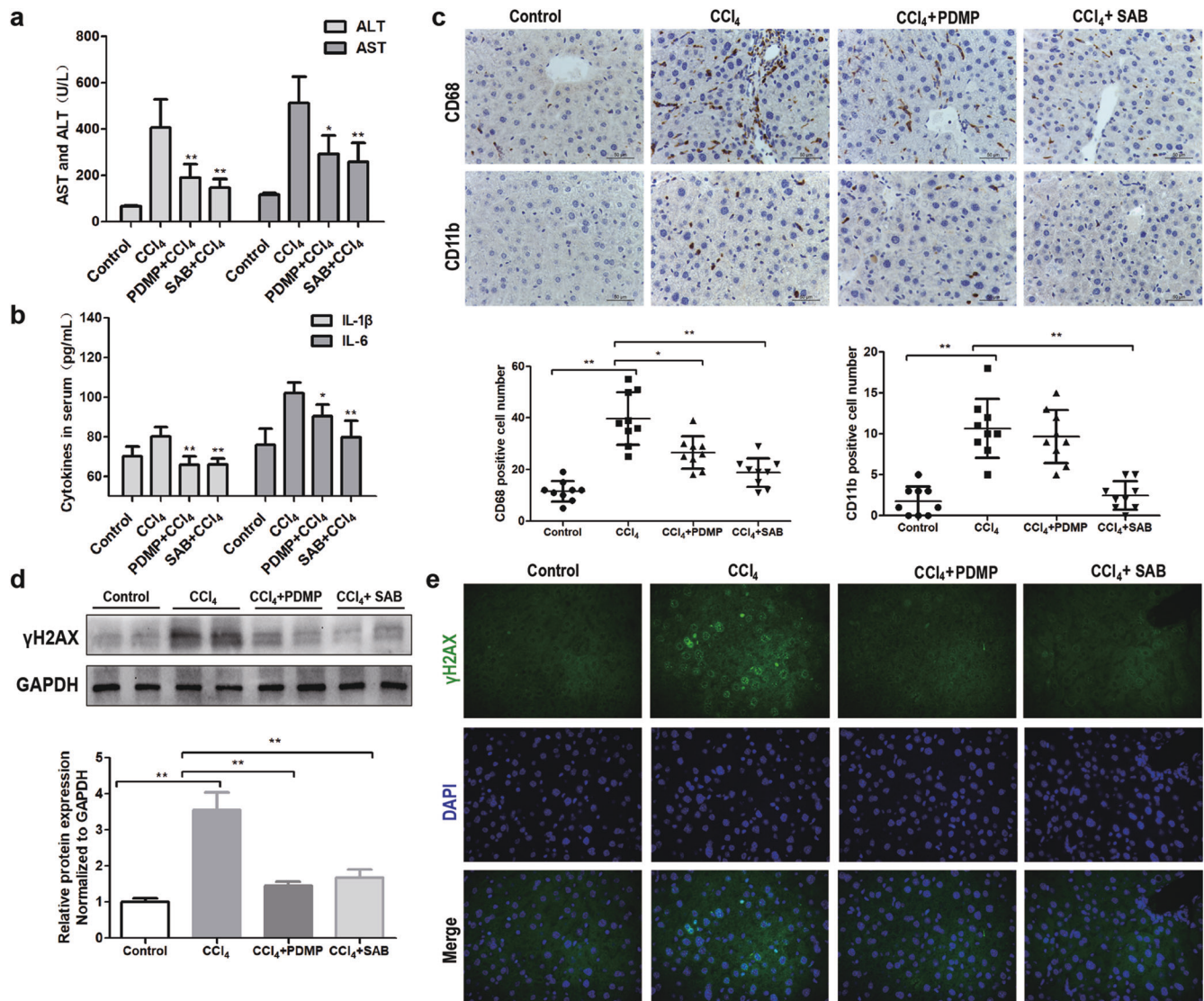
Salvianolic acid B suppresses hepatic fibrosis by inhibiting UGCG
ZB Li et al.

1203

Fig. 9 Effects of PDMP and SAB on liver injury and inflammation. a The concentrations of ALT and AST in mice serum. **b** The concentration of IL-1β and IL-6 in mice serum. **c** Immunohistochemical detection of CD68 and CD11b protein expression in mice liver tissues (40×, scale bar, 50 μm). **d** Relative protein levels of γH2AX in mice livers, as measured by Western blot. **e** The expression level of γH2AX was evaluated by immunofluorescence. The experiments were repeated three times, and statistical significance was determined by a t-test. *$P < 0.05$, **$P < 0.01$.

in *E. coli*, but could not be purified [41, 42]. We obtained UDPG binding domain of mouse UGCG for the first time, this would facilitate the research of the structure and of UDPG binding domain. We found that the aggregation state of UGCG was related to the redox state, the oxidation state of protein would affect the activation of HSCs. Some studies had also proved that ROS was related to the activation of HSCs [43, 44]. Aspartic acid, as a proton receptor, plays an essential role in the transglycosylation of a variety of glycosyltransferases [45]. The reaction mechanism and substrate specificity of UDP glucuronosyltransferase 1 A were mediated by aspartic acid [46], it was reported that D393A mutation abolished the glucuronidation activity of UGT1A10 toward all substrates [47]. A recent report showed that Asp553 of α-1,4-Glucan Lyases acted as a nucleophile and attacked the anomeric carbon causing the cleavage of the glycosidic bond [48]. Our results showed that the mutation of D236 could lead to the complete loss of UGCG activity. In agreement with our results, a previous study showed that D236 was an important amino acid participating in catalytic reaction [49]. Besides, we used alphafold structure prediction to obtain the full-length structure of UGCG,

had a simple understanding of the protein structure and catalytic mechanism of UGCG.

The effective components of *Salvia miltiorrhiza*, including Salvianolic acids, Tanshinone and Salvianic acid A, and so on, have been reported to have significant antifibrotic effects [50–53]. SAB is the main active ingredient in the water-soluble extract of *Salvia miltiorrhiza* Bge, and used to treat cardiovascular and liver diseases [54, 55]. According to reports, SAB could regulate TGF-β, FGF/FGFR, MEF signaling pathways to inhibit the activation of HSCs [56–58], indicating that SAB is a potential drug candidate for the treatment of liver fibrosis. However, there was no target of SAB has been reported. Our experiment found that SAB could inhibit the activity of UGCG, which is the first inhibitor of UGCG from traditional Chinese medicine. We verified the anti-fibrosis activity of SAB in vitro and in vivo. However, our experiments show that UGCG was the target of SAB against liver fibrosis, but it is not the main target, the main target of SAB against liver fibrosis still needs further research. In addition, SAB also showed good anti-inflammatory activity and could inhibit the activation of Kuffer cells, the anti-inflammatory effect of SAB still needs to be further

1204

explored. Our findings will help clinical research on drug development and pathological mechanisms.

AUTHOR CONTRIBUTIONS
ZBL and LJ performed the experiments; SGW, ZQL, and CYW designed the project and revised the paper; ZBL, LJ, JDN, YHX, FL, WML performed the informatics analysis and experiments; ZBL and CYW wrote the paper. All authors read and approved the final paper.

ADDITIONAL INFORMATION
Competing interests: The authors declare no competing interests.

REFERENCES
1. Novo E, Parola M. The role of redox mechanisms in hepatic chronic wound healing and fibrogenesis. Fibrogenes Tissue Repair. 2012;5:S4.
2. Zhang CY, Yuan WG, He P, Lei JH, Wang CX. Liver fibrosis and hepatic stellate cells: etiology, pathological hallmarks and therapeutic targets. World J Gastroenterol. 2016;22:10512–22.
3. Kisseleva T, Brenner D. Molecular and cellular mechanisms of liver fibrosis and its regression. Nat Rev Gastroenterol Hepatol. 2021;18:151–66.
4. Tsuchida T, Friedman SL. Mechanisms of hepatic stellate cell activation. Nat Rev Gastroenterol Hepatol. 2017;14:397–411.
5. Ezhilarasan D, Sokal E, Najimi M. Hepatic fibrosis: It is time to go with hepatic stellate cell-specific therapeutic targets. Hepatobiliary Pancreat Dis Int. 2018;17:192–7.
6. Trivedi P, Wang S, Friedman SL. The power of plasticity-metabolic regulation of hepatic stellate cells. Cell Metab. 2021;33:242–57.
7. Mao YQ, Fan XM. Autophagy: A new therapeutic target for liver fibrosis. World J Hepatol. 2015;7:1982–6.
8. Gao J, Wei B, de Assuncao TM, Liu Z, Hu X, Ibrahim S, et al. Hepatic stellate cell autophagy inhibits extracellular vesicle release to attenuate liver fibrosis. J Hepatol. 2020;73:1144–54.
9. Thoen LF, Guimaraes EL, Dolle L, Mannaerts I, Najimi M, Sokal E, et al. A role for autophagy during hepatic stellate cell activation. J Hepatol. 2011;55:1353–60.
10. Hong Y, Li S, Wang J, Li Y. In vitro inhibition of hepatic stellate cell activation by the autophagy-related lipid droplet protein ATG2A. Sci Rep. 2018;8:9232.
11. Hernandez-Gea V, Hilscher M, Rozenfeld R, Lim MP, Nieto N, Werner S, et al. Endoplasmic reticulum stress induces fibrogenic activity in hepatic stellate cells through autophagy. J Hepatol. 2013;59:98–104.
12. Tuohetahuntila M, Molenaar MR, Spee B, Brouwers JF, Wubbolts R, Houweling M, et al. Lysosome-mediated degradation of a distinct pool of lipid droplets during hepatic stellate cell activation. J Biol Chem. 2017;292:12436–48.
13. Lee TF, Mak KM, Rackovsky O, Lin YL, Kwong AJ, Loke JC, et al. Downregulation of hepatic stellate cell activation by retinol and palmitate mediated by adipose differentiation-related protein (ADRP). J Cell Physiol. 2010;223:648–57.
14. Jing XY, Yang XF, Qing K, Ou-yang Y. Roles of the lipid metabolism in hepatic stellate cells activation. Chin Med Sci J. 2013;28:233–6.
15. Schomel N, Gruber L, Alexopoulos SJ, Trautmann S, Olzomer EM, Byrne FL, et al. UGCG overexpression leads to increased glycolysis and increased oxidative phosphorylation of breast cancer cells. Sci Rep. 2020;10:8182.
16. Schomel N, Hancock SE, Gruber L, Olzomer EM, Byrne FL, Shah D, et al. UGCG influences glutamine metabolism of breast cancer cells. Sci Rep. 2019;9:15665.
17. Schomel N, Geisslinger G, Wegner MS. Influence of glycosphingolipids on cancer cell energy metabolism. Prog Lipid Res. 2020;79:101050.
18. Li Z, Zhang L, Liu D, Wang C. Ceramide glycosylation and related enzymes in cancer signaling and therapy. Biomed Pharmacother. 2021;139:111565.
19. Zhuo D, Li X, Guan F. Biological roles of aberrantly fxpressed glycosphingolipids and related enzymes in human cancer development and progression. Front Physiol. 2018;9:466.
20. Guri Y, Colombi M, Dazert E, Hindupur SK, Roszik J, Moes S, et al. mTORC2 promotes tumorigenesis via lipid synthesis. Cancer Cell. 2017;32:807–23.e12.
21. Jennemann R, Federico G, Mathow D, Rabionet M, Rampoldi F, Popovic ZV, et al. Inhibition of hepatocellular carcinoma growth by blockade of glycosphingolipid synthesis. Oncotarget. 2017;8:109201–16.
22. Bangen JM, Hammerich L, Sonntag R, Baues M, Haas U, Lambertz D, et al. Targeting CCl$_4$-induced liver fibrosis by RNA interference-mediated inhibition of cyclin E1 in mice. Hepatology. 2017;66:1242–57.
23. Tao XM, Li D, Zhang C, Wen GH, Wu C, Xu YY, et al. Salvianolic acid B protects against acute and chronic liver injury by inhibiting Smad2C/L phosphorylation. Exp Ther Med. 2021;21:341.
24. Modak RV, Zaiss DM. Isolation and culture of murine hepatic stellate cells. Bio Protoc. 2019;9:e3422.
25. Fenderson BA, Ostrander GK, Hausken Z, Radin NS, Hakomori S. A ceramide analogue (PDMP) inhibits glycolipid synthesis in fish embryos. Exp Cell Res. 1992;198:362–6.
26. Zhong B, Liu M, Bai C, Ruan Y, Wang Y, Qiu L, et al. Caspase-8 induces lysosome-associated cell death in cancer cells. Mol Ther. 2020;28:1078–91.
27. Li Z, Chiang YP, He M, Worgall TS, Zhou H, Jiang XC. Liver sphingomyelin synthase 1 deficiency causes steatosis, steatohepatitis, fibrosis, and tumorigenesis: An effect of glucosylceramide accumulation. iScience. 2021;24:103449.
28. Iredale JP, Thompson A, Henderson NC. Extracellular matrix degradation in liver fibrosis: Biochemistry and regulation. Biochim Biophys Acta. 2013;1832:876–83.
29. Ortiz C, Schierwagen R, Schaefer L, Klein S, Trepat X, Trebicka J. Extracellular matrix remodeling in chronic liver disease. Curr Tissue Microenviron Rep. 2021;2:41–52.
30. Roderfeld M. Matrix metalloproteinase functions in hepatic injury and fibrosis. Matrix Biol. 2018;68-69:452–62.
31. Zhang J, Jiang N, Ping J, Xu L. TGF-β1-induced autophagy activates hepatic stellate cells via the ERK and JNK signaling pathways. Int J Mol Med. 2021;47:256–66.
32. Deng J, Huang Q, Wang Y, Shen P, Guan F, Li J, et al. Hypoxia-inducible factor-1alpha regulates autophagy to activate hepatic stellate cells. Biochem Biophys Res Commun. 2014;454:328–34.
33. Chen M, Liu J, Yang W, Ling W. Lipopolysaccharide mediates hepatic stellate cell activation by regulating autophagy and retinoic acid signaling. Autophagy. 2017;13:1813–27.
34. Myerowitz R, Puertollano R, Raben N. Impaired autophagy: The collateral damage of lysosomal storage disorders. EBioMedicine. 2021;63:103166.
35. Koike K, Berdyshev EV, Mikosz AM, Bronova IA, Bronoff AS, Jung JP, et al. Role of glucosylceramide in lung endothelial cell fate and emphysema. Am J Respir Crit Care Med. 2019;200:1113–25.
36. Bodas M, Min T, Vij N. Lactosylceramide-accumulation in lipid-rafts mediate aberrant-autophagy, inflammation and apoptosis in cigarette smoke induced emphysema. Apoptosis. 2015;20:725–39.
37. Hartwig P, Hoglinger D. The glucosylceramide synthase inhibitor PDMP causes lysosomal lipid accumulation and mTOR inactivation. Int J Mol Sci. 2021;22:7065.
38. Feng J, Chen K, Xia Y, Wu L, Li J, Li S, et al. Salidroside ameliorates autophagy and activation of hepatic stellate cells in mice via NF-kappaB and TGF-β1/Smad3 pathways. Drug Des Devel Ther. 2018;12:1837–53.
39. Ji J, Yu Q, Dai W, Wu L, Feng J, Zheng Y, et al. Apigenin alleviates liver fibrosis by inhibiting hepatic stellate cell activation and autophagy via TGF-β1/Smad3 and p38/PPARalpha Pathways. PPAR Res. 2021;2021:6651839.
40. Meng D, Li Z, Wang G, Ling L, Wu Y, Zhang C. Carvedilol attenuates liver fibrosis by suppressing autophagy and promoting apoptosis in hepatic stellate cells. Biomed Pharmacother. 2018;108:1617–27.
41. Ichikawa S, Sakiyama H, Suzuki G, Hidari KI, Hirabayashi Y. Expression cloning of a cDNA for human ceramide glucosyltransferase that catalyzes the first glycosylation step of glycosphingolipid synthesis. Proc Natl Acad Sci USA. 1996;93:4638–43.
42. Ichikawa S, Ozawa K, Hirabayashi Y. Molecular cloning and expression of mouse ceramide glucosyltransferase. Biochem Mol Biol Int. 1998;44:1193–202.
43. Ramos-Tovar E, Muriel P. Molecular mechanisms that link oxidative stress, inflammation, and fibrosis in the liver. Antioxidants (Basel). 2020;9:1279.
44. Lu C, Zou Y, Liu Y, Niu Y. Rosmarinic acid counteracts activation of hepatic stellate cells via inhibiting the ROS-dependent MMP-2 activity: Involvement of Nrf2 antioxidant system. Toxicol Appl Pharmacol. 2017;318:69–78.
45. Shibayama K, Ohsuka S, Sato K, Yokoyama K, Horii T, Ohta M. Four critical aspartic acid residues potentially involved in the catalytic mechanism of Escherichia coli K-12 WaaR. FEMS Microbiol Lett. 1999;174:105–9.
46. Li D, Fournel-Gigleux S, Barre L, Mulliert G, Netter P, Magdalou J, et al. Identification of aspartic acid and histidine residues mediating the reaction mechanism and the substrate specificity of the human UDP-glucuronosyltransferases 1A. J Biol Chem. 2007;282:36514–24.
47. Xiong Y, Patana AS, Miley MJ, Zielinska AK, Bratton SM, Miller GP, et al. The first aspartic acid of the DQxD motif for human UDP-glucuronosyltransferase 1A10 interacts with UDP-glucuronic acid during catalysis. Drug Metab Dispos. 2008;36:517–22.
48. Campesato L, Marforio TD, Giacinto P, Calvaresi M, Bottoni A. A full QM computational study of the catalytic mechanism of alpha-1,4-glucan lyases. Chemphyschem. 2018;19:1514–21.

Salvianolic acid B suppresses hepatic fibrosis by inhibiting UGCG
ZB Li et al.

1205

49. Wu K, Marks DL, Watanabe R, Paul P, Rajan N, Pagano RE. Histidine-193 of rat glucosylceramide synthase resides in a UDP-glucose- and inhibitor (D-threo-1-phenyl-2-decanoylamino-3-morpholinopropan-1-ol)-binding region: a biochemical and mutational study. Biochem J. 1999;341:395–400.

50. Tsai MK, Lin YL, Huang YT. Effects of salvianolic acids on oxidative stress and hepatic fibrosis in rats. Toxicol Appl Pharmacol. 2010;242:155–64.

51. Wang R, Song F, Li S, Wu B, Gu Y, Yuan Y. Salvianolic acid A attenuates CCl_4-induced liver fibrosis by regulating the PI3K/AKT/mTOR, Bcl-2/Bax and caspase-3/cleaved caspase-3 signaling pathways. Drug Des Devel Ther. 2019;13:1889–900.

52. Shi MJ, Yan XL, Dong BS, Yang WN, Su SB, Zhang H. A network pharmacology approach to investigating the mechanism of Tanshinone IIA for the treatment of liver fibrosis. J Ethnopharmacol. 2020;253:112689.

53. Lan Y, Yan R, Shan W, Chu J, Sun R, Wang R, et al. Salvianic acid A alleviates chronic alcoholic liver disease by inhibiting HMGB1 translocation via down-regulating BRD4. J Cell Mol Med. 2020;24:8518–31.

54. Xiao Z, Liu W, Mu YP, Zhang H, Wang XN, Zhao CQ, et al. Pharmacological effects of salvianolic acid B against oxidative damage. Front Pharmacol. 2020;11:572373.

55. Li CL, Liu B, Wang ZY, Xie F, Qiao W, Cheng J, et al. Salvianolic acid B improves myocardial function in diabetic cardiomyopathy by suppressing IGFBP3. J Mol Cell Cardiol. 2020;139:98–112.

56. Tao YY, Wang QL, Shen L, Fu WW, Liu CH. Salvianolic acid B inhibits hepatic stellate cell activation through transforming growth factor beta-1 signal transduction pathway in vivo and in vitro. Exp Biol Med (Maywood). 2013;238:1284–96.

57. Tian S, Chen M, Wang B, Han Y, Shang H, Chen J. Salvianolic acid B blocks hepatic stellate cell activation via FGF19/FGFR4 signaling. Ann Hepatol. 2021;20:100259.

58. Zhang W, Ping J, Zhou Y, Chen G, Xu L. Salvianolic acid B inhibits activation of human primary hepatic stellate cells through downregulation of the myocyte enhancer factor 2 signaling pathway. Front Pharmacol. 2019;10:322.